

Advanced Series Resistance Imaging for Silicon Solar Cells via Electroluminescence

Georg Dost,* Hannes Höffler, and Johannes M. Greulich

Herein, a method for advanced series resistance imaging via electroluminescence (EL) for silicon solar cells is presented. The well-known method by Haunschild et al. is revisited. The Fuyuki assumption of a linear relation between diffusion length and EL signal is shown to be not applicable to silicon devices nowadays due to larger minority charge carrier diffusion lengths and thinner solar cells. A new relation derived by Breitenstein is used here instead. The updated method for series resistance and saturation current imaging based on two EL images, which show a far superior separation of contrast and almost 60% shorter data acquisition times in comparison with the original method by Haunschild, is presented. The Weber contrast of the unwanted signal caused by recombination in resistance image is reduced from 0.89 to 0.44, using the advanced method for a prominent feature on the sample cell. The contrast due to resistance stays at the same level. The dark saturation current density images show 20% higher peaks at recombination active areas and also a 5% low.

1. Introduction

Electroluminescence (EL) imaging is a long-established technology for solar cell characterization.^[1,2] Areas with lower densities of excess charge carriers show lower signals in the resulting image. The reasons for these reduced densities are manifold. For an easier identification of the problems of the solar cell, be it by hand, classic pattern recognition techniques, or by machine learning approaches, a separation of contrasts in an EL image is helpful. One approach is to separate contrast caused by series resistance on the one hand and recombination in the bulk material on the other. Series resistance is an important property to investigate in a spatially resolved manner. That is because the defects increasing it are usually very

inhomogeneously distributed over the cell. The examples are problems during firing that lead to faulty contact forming, problems during screen printing, or finger defects.

There are different approaches to separate contrasts of a luminescence image based on the model of independent diodes.^[3–5] Other approaches use inhomogeneous illumination^[6,7] or lock-in photoluminescence^[8] but require additional hardware. Methods^[9,10] that refrain from using the model of independent diodes are complex and not mature yet.^[11] The coupled determination of dark saturation current and series resistance (C-DCR)^[12] shows a very clear separation of contrasts but requires the measurement setup to be able to perform photoluminescence imaging. Another method is the ‘series

resistance EL’ (R_s EL) by Haunschild et al.^[13] It was improved on by Breitenstein using iteration (iterating R_s EL).^[14] These fast series resistance imaging techniques are further developed into “nonlinear R_s EL” to meet the requirements of ever thinner solar cells with higher lifetimes in this article.

2. Theory

The following methods utilize the model of independent diodes, i.e., every image pixel is connected to the terminal via an independent series resistance. While this holds true for samples with a homogeneous dark saturation current density j_0 , it leads to errors for cells with varying j_0 due to lateral balancing currents. It is overall a well working approximation though, that is much simpler than more complex models with distributed series resistance and therefore used.


At low voltages, the lateral currents on solar cells are so low that a voltage variation much smaller than the thermal voltage $U_t = 25.6$ mV across the surface of the cell can be assumed at room temperature. A calibration factor C_i for each pixel i can then be derived using the exponential relation between the EL signal $\Phi_{i,i}$ of an image taken at a low applied voltage U_l .

$$C_i = \Phi_{i,i} / \exp[U_l / U_t] \quad (1)$$

with U_t being the thermal voltage.

Now the EL signal $\Phi_{h,i}$ of a second image taken at a high voltage can be calibrated to local voltage $U_{h,i}$ using the same equation

G. Dost, Dr. H. Höffler, Dr. J. M. Greulich
 Division Photovoltaics
 Fraunhofer Institute for Solar Energy Systems
 Heidenhofstraße 2, Freiburg im Breisgau 79110, Germany
 E-mail: georg.dost@ise.fraunhofer.de

 The ORCID identification number(s) for the author(s) of this article can be found under <https://doi.org/10.1002/pssa.202000546>.

© 2021 The Authors. physica status solidi (a) applications and materials science published by Wiley-VCH GmbH. This is an open access article under the terms of the Creative Commons Attribution-NonCommercial License, which permits use, distribution and reproduction in any medium, provided the original work is properly cited and is not used for commercial purposes.

DOI: 10.1002/pssa.202000546

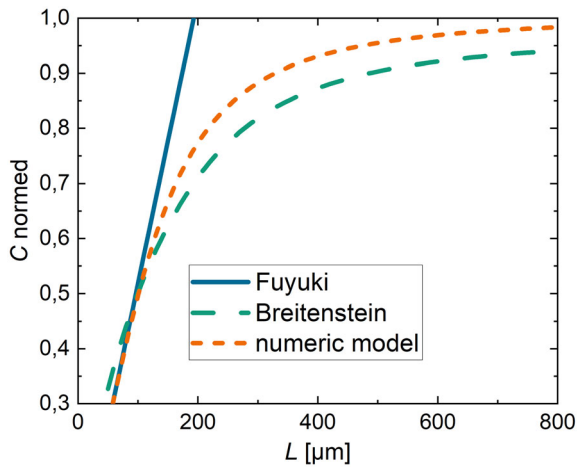


Figure 1. This graph shows the relation between the diffusion length L and therefore j_0 and the normalized calibration factor C . The solid line shows linear approximation for j_0 by Fuyuki as used in Haunschild's method. The dashed line shows the approximation by Breitenstein. Here C_{\max} is chosen to match the numeric model toward infinite length L . The dotted line shows a 1D numeric model for calculating the number of electrons in the bulk using a finite width of $200\ \mu\text{m}$, a diffusion coefficient of $32\ \text{cm}^2\ \text{s}^{-1}$, and a rear surface recombination velocity of $100\ \text{cm}\ \text{s}^{-1}$.

$$U_{h,i} = U_t \ln \left[\frac{\Phi_{h,i}}{C_i} \right] \quad (2)$$

The series resistance is in this work defined as the resistance that causes the drop of local voltage $U_{h,i}$ in comparison with the applied voltage U_h .

$$R_{s,i} = \frac{U_h - U_{h,i}}{j_{h,i}} = \frac{U_h - U_{h,i}}{j_{0,i} \exp[U_{h,i}/U_t]} \quad (3)$$

with $j_{h,i}$ being the current density and $j_{0,i}$ being the dark saturation current density.

Haunschild et al.^[13] used a linear approximation by Fuyuki^[2] that states $j_{0,i} \approx 1/L \approx 1/C_i$. But this linear relation between the two quantities is derived under the assumption that the width of the cell W is much larger than the charge carriers' diffusion length $L \ll W$. This assumption is not valid anymore in modern silicon solar cells, as shown in Section 3. Therefore, a 1D model (neglecting emitter, assuming constant minority charge carrier lifetime, derived by solving the diffusion equation) featuring a finite width W and recombination at the back surface S of the solar cell was calculated by integrating the depth distribution of the charge carriers under bias. This leads to

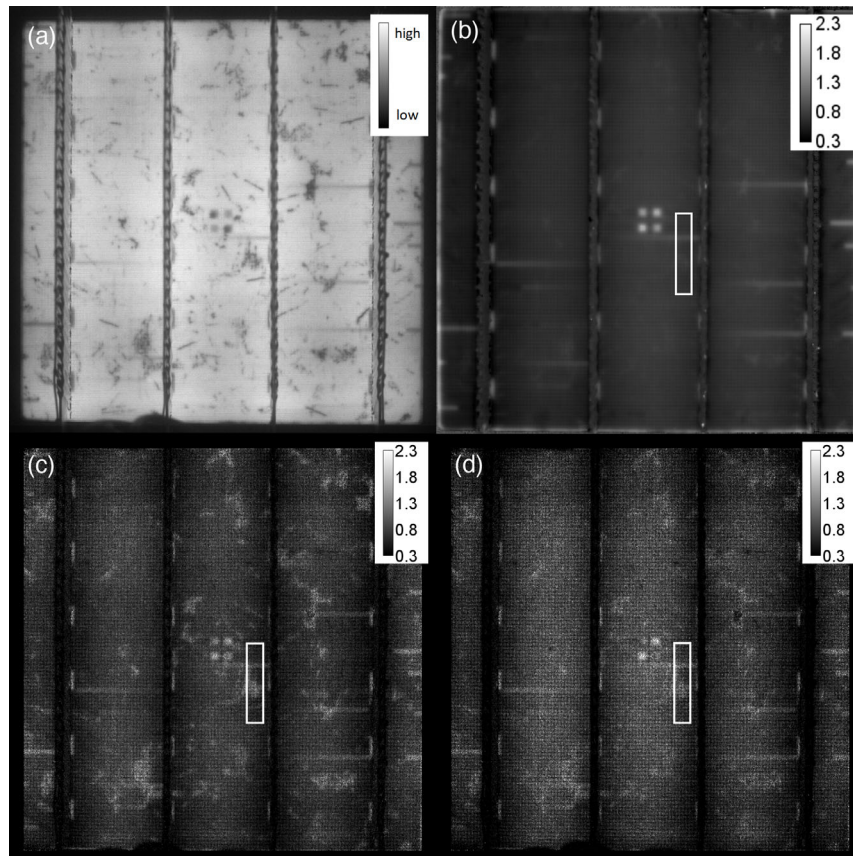


Figure 2. a) Contrast EL image of mc-PERC solar cell. b) R_s image in Ωcm^2 determined by C-DCR as the quality goal. c) R_s image in Ωcm^2 determined by the iterating R_s EL method, d) R_s image in Ωcm^2 determined by the nonlinear R_s EL method. Artifacts due to recombination are much more strongly visible using the iterating R_s EL, whereas the contrast of resistance-induced effects stays the same. Profiles along the boxes in the lower images are shown in Figure 3.

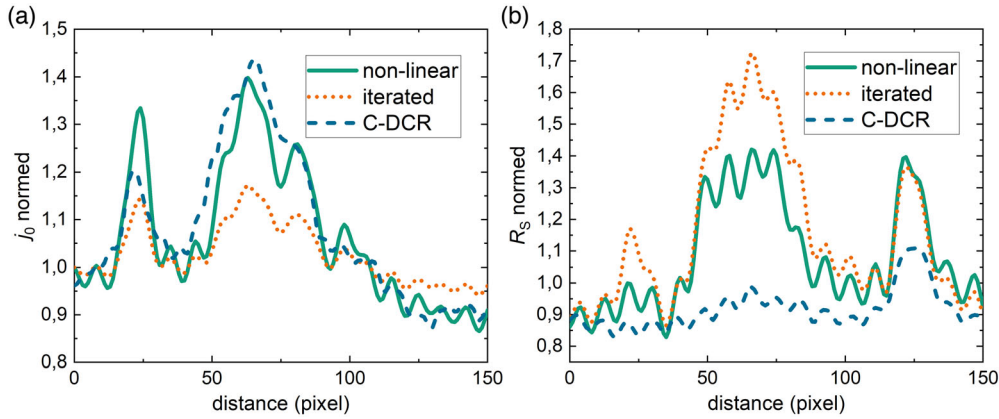


Figure 3. a) The profile of R_s along the boxes in Figure 2b–d from the top to bottom for the iterating R_s EL, the nonlinear R_s EL, and C-DCR normalized on the baseline around 5 pixel. The graphs of the nonlinear method and C-DCR match up well considering the different camera type and resolution of the C-DCR data. b) The profile of j_0 along the boxes in Figure 4b–d for the iterating R_s EL, the nonlinear R_s EL, and C-DCR. The dislocation cluster from 50 to 80 pixels shows a much stronger j_0 in the nonlinear method. The unwanted contrast of this cluster is strongly reduced in the resistance image. The contrast of the finger defect at 125 pixels remains the same for both images. While the small scratch at 25 pixels is completely removed from the resistance image, the bigger dislocation cluster's Weber contrast is reduced to 0.44 by 0.89. C-DCR removes the unwanted contrast completely.

$$C \sim L \frac{1 - \frac{D}{SL} + \frac{2D}{SL} \exp\left[\frac{W}{L}\right]}{\frac{D}{SL} - 1 + \left(1 + \frac{D}{SL}\right) \exp\left[\frac{2W}{L}\right]} \quad (4)$$

with D as the diffusion coefficient of the minority charge carriers, i.e., electrons in p-type solar cells. This relation is in the following called numeric model. It is not analytically solvable and therefore takes too much time to solve for every pixel for an inline application. Furthermore D , S , and L have to be known.

Because of that, another approximation, that has a saturation value C_{\max} , is used here, as derived by Breitenstein et al.^[15]

$$j_{0,i} \approx \frac{1 - C_i/C_{\max}}{C_i/C_{\max}} \quad (5)$$

Breitenstein uses light beam induced current measurements to identify C_{\max} . To make it an independent method, here, C_{\max} is instead found by varying it and finding the one that corresponds with the best separation of contrasts in the resulting j_0 and R_s by human rating. The found C_{\max} will be used for all solar cells that are processed identically. As C_i relates the measured voltage to the values measured by the luminescence camera, optical factors changing the path of luminescence radiation are included in it. This includes optical artifacts like vignetting,^[16,17] which therefore have to be corrected in the raw EL images prior to calculations.

In **Figure 1**, the different relations between a normalized correlation constant $C_{x,\text{normalized}}$

$$C_{x,\text{normalized}} = C_x(L)/C_{1d\text{ model}}(L = \infty) \quad (6)$$

and the diffusion length L and therefore j_0 are shown. The index x stands for the different relations that are used to calculate C : “Fuyuki,” “Breitenstein,” and the “numeric model.” These are the different relations to approximate j_0 , based on the correlation constant. It is seen that only for small L the linear relation by Fuyuki yields similar results to the others. Breitenstein's

equation is in contrast to the numeric model analytically solvable and therefore much faster to use. It seems to underestimate c in comparison with the numeric model if the same maximum is assumed, as shown in **Figure 1**. Therefore C_{\max} is optimized as described earlier and without the use of lifetime and surface recombination velocities to keep the method easy to use.

An image taken at low voltages needs high exposure times to collect sufficient intensity. To accelerate the method, Breitenstein et al. suggested an iterative approach that is also part of the method presented here.^[14] Here, instead of abiding the assumption that an image taken at a low terminal voltage has constant voltage across the image, the image is taken at higher voltages. The advantage is the shorter exposure time necessary for a good signal-to-noise ratio and therefore the ability to be used in industrial-scale characterization. Doing so leads to an error in the first iteration of the resulting series resistance. Therefore, for the next iteration, a spatially resolved lower voltage $U_{l,i}$ is calculated by

$$U_{l,i}^{k+1} = U_l - R_{s,i} j_{0,i}^k \exp[U_{l,i}^k/U_t] \quad (7)$$

and used in Equation (1). After a few iterations of Equations (1)–(3), the series resistance converges.

As the approximation for $j_{0,i}$ is a proportionality and not an equation, the determined dark saturation current density and series resistance are in the first place contrast images only. To obtain quantitative images a scaling factor f can be found by comparing the mean value of the unscaled R_s image with a global R_s value found by fitting the two-diode model to the I – V curve of the cell measured under illumination.^[14]

$$\begin{aligned} f &= \frac{R_{s,\text{global}}}{R_{s,i,\text{co}}} \\ R_{s,i} &= f R_{s,i,\text{co}} \\ j_{0,i} &= j_{0,i,\text{co}}/f \end{aligned} \quad (8)$$

where the index “co” refers to the unscaled contrast images.

The approach including the iteration and the nonlinear replacement of the Fuyuki approximation by Breitenstein et al. [15] is referred to as “nonlinear R_s EL,” whereas the approach including the iteration and the original Fuyuki approximation is referred to as “iterating R_s EL.”

3. Method

Two EL images at different biases have to be taken. The higher current should not exceed currents in the solar cell under working conditions too far. The lower current should be chosen as high as possible to save time and as low as necessary for the method to show clear results. In this work, 6 and 10 A have been used.

Using the image taken at lower bias, the correlation constant C_i is calculated via Equation (1).

The image taken at a higher bias is calibrated to voltage using C_i and Equation (2).

A first iteration of the series resistance $R_{s,i}$ is calculated by Equation (3) using Equation (5) as an approximation of j_0 . The value of C_{max} is approximated for now as the highest value of C_i appearing in the image.

Using Equation (7), a more precise image of the voltage of the image taken at a lower bias is calculated. With these new values for the lower voltage, the procedure is now iterated over Equations (1), (2), (5), (3), and (7), until the series resistance results of Equation (3) converge and do not change anymore.

Now C_{max} has to be optimized by iterating the whole method until the contrast separation shows best results by human rating. This was done by automatizing the method and using a slider to vary C_{max} . This has to be done only once and can then be used for a batch of the same solar cells. A cell with an R_s defect like a finger defect, ideally close to the center and not at the edges of the cell, should be used. C_{max} is chosen optimally when the contrast of the finger defect with its surroundings is maximal. Deviating from this maximum in both directions will lower the contrast of the finger defect.

The last step is scaling the images of $j_{0,i}$ and $R_{s,i}$ via Equation (8) and a known global value for R_s .

4. Results and Discussion

In **Figure 2**, an EL and several R_s images of a passivated emitter and rear cell (PERC) based on multicrystalline (mc) silicon are

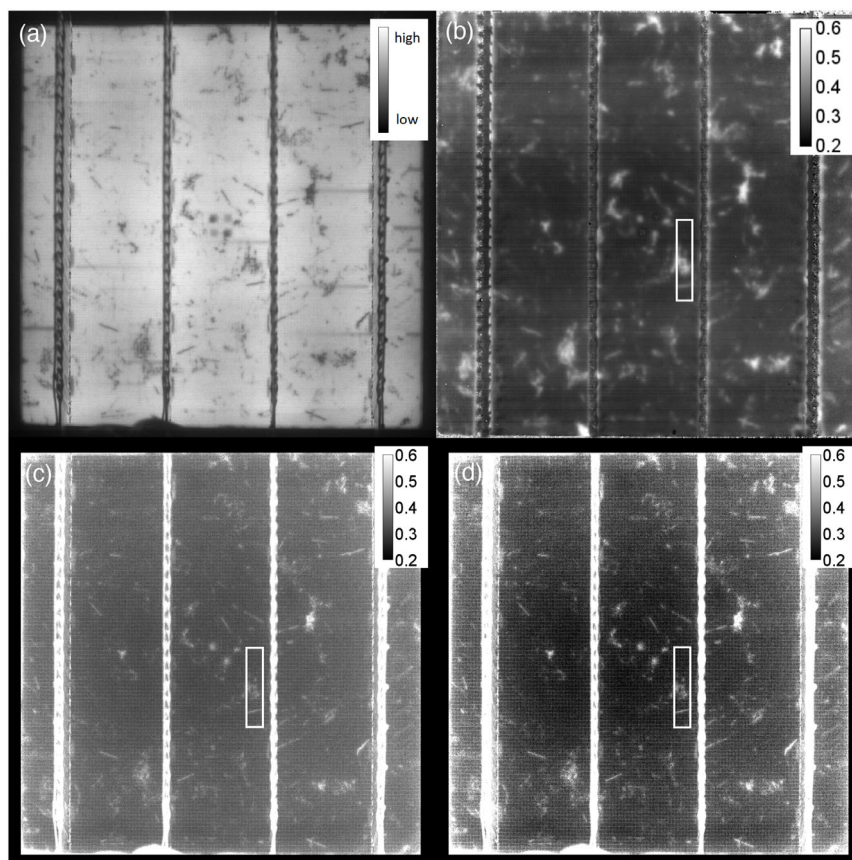


Figure 4. a) Contrast EL image of the same mc-PERC solar cell as in Figure 2. b) j_0 image in pA/cm^2 determined by C-DCR as the quality goal. c) j_0 image in pA/cm^2 determined by the iterating R_s EL method. d) j_0 image in pA/cm^2 determined by the nonlinear R_s EL method. The current density values in (c) and (d) are gained by scaling with a global value. The peaks of the dislocation clusters and other recombination active defects are much stronger in the new method. Therefore, the iterating R_s EL method shows higher values for areas of defect-free material. The C-DCR image has a much smaller resolution and seems therefore blurry in comparison. Profiles along the boxes in the lower images are shown in Figure 3.

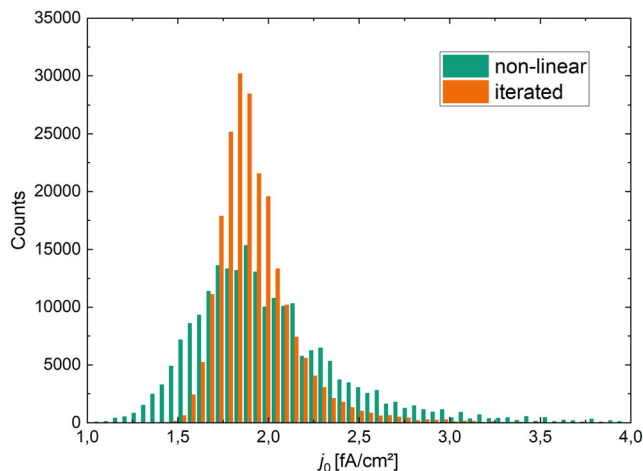


Figure 5. Histogram of the j_0 images in Figure 4c,d created by the iterating R_s EL and the nonlinear R_s EL method, respectively. The new, nonlinear method has a broader histogram. The “good” areas of the cell have lower values whereas the peaks at the dislocation clusters have higher values, thus stretching the histogram.

shown. It has an efficiency of 18.6%, a width W of 197 μm , and a global series resistance of $0.64 \Omega\text{cm}^2$. The cell size is 156 mm \times 156 mm. A two-diode fit of the I – V characteristics yields $j_{01} = 390 \text{ fA/cm}^2$. Using the equation

$$L_{\text{eff}} = \frac{eDn_i^2}{N_{\text{Dop}}j_{01}} \quad (9)$$

With e as the elementary charge, the diffusion coefficient $D = 32 \text{ cm}^2\text{s}^{-1}$,^[18] the intrinsic charge carrier density $n_i = \frac{8.2e9}{\text{cm}^3}$,^[19] and the doping concentration $N_{\text{Dop}} = 4.85e15 \text{ cm}^{-3}$. This gives an effective diffusion length of 1820 μm . Therefore, the assumption of $W \gg L_{\text{eff}}$ does not hold for this solar cell. The images for the EL-based methods were taken at 669.2 mV and 634.1 mV, respectively, with a Si charge-coupled device camera for 0.3 and 0.7 s, respectively, and the iteration was applied. With 2×2 pixel binning, the sum of the exposure times decreases to 275 ms, clearly at the cost of a reduced resolution. No short-pass filter is used in this setup. This could improve the image quality by suppressing photon smearing in the sample and the detector. Approximation (5) also would be matched better but at the cost of measuring time.^[14]

In the EL image, material effects like dislocation clusters, but also resistance effects as finger defects, are seen as contrast. C-DCR, a luminescence method based on illumination, is used here for comparison and as a goal to get close to R_s EL that works without illumination.

In the R_s image in (c) calculated by the iterating R_s EL method, strong and unwanted material-based contrasts are visible. These are strongly reduced by the new method, as shown in Figure 2d. The Weber contrast K_w of the intensity between two points is generally defined as $K_w = I_{\text{high}}/I_{\text{low}} - 1$. While the contrasts caused by smaller areas of recombination are completely removed from the resistance image, the bigger dislocation cluster’s Weber contrast is reduced to 0.44 from 0.89 using the peak signal and the average of the surrounding base signal in

Figure 3b. The contrast of the resistance effects stays at the same level. The slightly higher series resistance between the bus bars in the middle of the image is due to the imperfect correction of the vignetting artifact.

In **Figure 4**, the same EL image and the corresponding j_0 images are shown. The contrast images c) and d), created by the iterating and nonlinear R_s EL method, show similar contrasts. But being scaled with a global value, differences become apparent. The peaks of the dislocation clusters and other recombination active defects are much stronger with the new method. Therefore the iterating R_s EL method shows higher values for “good” material. This is seen in the histograms of the images in Figure 4c,d shown in **Figure 5**.

There are still material-based contrasts seen in the R_s image of the nonlinear method. One reason is the relation between j_0 and the calibration factor C after Breitenstein et al. It is still only an approximation and also derived for the special case of low luminescence wavelength between 950 and 1000 nm. In the used EL setup, no filters are used to accelerate image capture.

5. Conclusion

To avoid approximations in series resistance imaging that cause bigger errors with better-performing solar cells, the fast series resistance imaging of Haunschild is updated. The approximation for the dark saturation current density is changed to a saturating function by Breitenstein to fit thin solar cells with high lifetimes and is adjusted to be used independently of other measurement devices. Because of this, the contrast separation of series resistance-related effects and material-related effects is improved: The Weber contrast of an exemplary dark spot caused by recombination in the series resistance image dropped from 0.88 to 0.44. An iterative approach was used, accelerating the measurement and thus enabling the application of this method for inline testing, reducing the exposure time of the second image from 2 s to 0.7 s in maximal resolution for an older mc-PERC cell ($V_{\text{oc}} = 649 \text{ mV}$). With 2×2 pixel binning, the exposure time decreases to 275 ms. The required images differ only in the voltage at which the second image is taken. The equipment needed stays the same, but the contrast separation of series resistance effects on the one hand and material effects on the other hand is greatly enhanced.

Acknowledgements

This work was supported in part by the Federal Ministry for Economic Affairs and Energy (BMWi) under iMage-Project, contract number 0324045A. Open access funding enabled and organized by Projekt DEAL.

Conflict of Interest

The authors declare no conflict of interest.

Data Availability Statement

Research data are not shared.

Keywords

characterizations, electroluminescences, series resistances, silicon solar cells

Received: August 27, 2020

Revised: January 12, 2021

Published online: January 26, 2021

- [1] P. Würfel, T. Trupke, T. Puzzer, E. Schäffer, W. Warta, S. W. Glunz, *J. Appl. Phys.* **2007**, 101, 12.
- [2] T. Fuyuki, H. Kondo, T. Yamazaki, Y. Takahashi, Y. Uraoka, *Appl. Phys. Lett.* **2005**, 86, 26.
- [3] D. Hinken, K. Ramspeck, K. Bothe, B. Fischer, R. Brendel, *Appl. Phys. Lett.* **2007**, 91, 18.
- [4] H. Kampwerth, T. Trupke, J. W. Weber, Y. Augarten, *Appl. Phys. Lett.* **2008**, 93, 20.
- [5] T. Trupke, E. Pink, R. A. Bardos, M. Abbott, *Appl. Phys. Lett.* **2007**, 90, 9.
- [6] I. Zafirovska, M. K. Juhl, J. W. Weber, J. Wong, T. Trupke, *IEEE J. Photovoltaics* **2017**, 7, 6.
- [7] M. Kasemann, L. M. Reindl, B. Michl, W. Warta, A. Schütt, J. Carstensen, *IEEE J. Photovoltaics* **2012**, 2, 2.
- [8] P. Song, J. Liu, M. Oliullah, Y. Wang, *Phys. Status Solidi RRL* **2017**, 11, 7.
- [9] U. Rau, V. Huhn, L. Stoicescu, M. Schneemann, Y. Augarten, A. Gerber, B. E. Pieters, *Appl. Phys. Lett.* **2014**, 105, 16.
- [10] M. Glatthaar, J. Haunschild, R. Zeidler, M. Demant, J. Greulich, B. Michl, W. Warta, S. Rein, R. Preu, *J. Appl. Phys.* **2010**, 108, 1.
- [11] O. Breitenstein, J. Bauer, D. Hinken, K. Bothe, *Sol. Energy Mater. Sol. Cells* **2015**, 142, 92.
- [12] M. Glatthaar, J. Haunschild, M. Kasemann, J. Giesecke, W. Warta, S. Rein, *Phys. Status Solidi RRL* **2010**, 4, 7.
- [13] J. Haunschild, M. Glatthaar, M. Kasemann, S. Rein, E. R. Weber, *Phys. Status Solidi RRL* **2009**, 3, 7.
- [14] O. Breitenstein, A. Khanna, Y. Augarten, J. Bauer, J.-M. Wagner, K. Iwig, *Phys. Status Solidi RRL* **2010**, 4, 7.
- [15] O. Breitenstein, F. Frühauf, A. Teal, *IEEE J. Photovoltaics* **2016**, 6, 2.
- [16] K. Bedrich, M. Bokalic, M. Bliss, M. Topic, T. R. Betts, R. Gottschalg, *IEEE J. Photovoltaics* **2018**, 8, 5.
- [17] G. Dost, H. Höffler, J. M. Greulich, *Rev. Sci. Instr.* **2019**, 90, 10.
- [18] F. Schindler, M. Forster, J. Broisch, J. Schön, J. Giesecke, S. Rein, W. Warta, M. C. Schubert, *Sol. Energy Mater. Sol. Cells* **2014**, 131, 92.
- [19] K. Misiakos, D. Tsamakis, *J. Appl. Phys.* **1993**, 74, 5.